Active site voltage clamp fluorometry of the sodium glucose cotransporter hSGLT1

Edurne Gorraitz[a], Bruce A. Hirayama[a], Aviv Paz[a], Ernest M. Wright[a,1], and Donald D. F. Loo[a,1]

[a]Department of Physiology, David Geffen School of Medicine, University of California, Los Angeles, CA 90095-1751

Contributed by Ernest M. Wright, September 25, 2017 (sent for review August 7, 2017; reviewed by Francisco Bezanilla and Ian C. Forster)

In the human sodium glucose cotransporter (hSGLT1) cycle, the protein undergoes conformational changes where the sugar-binding site alternatively faces the external and internal surfaces. Functional site-directed fluorometry was used to probe the conformational changes at the sugar-binding site. Residues (Y290, T287, H83, and N78) were mutated to cysteines. The mutants were expressed in *Xenopus laevis* oocytes and tagged with environmentally sensitive fluorescent rhodamines [e.g., tetramethylrhodamine (TMR)-thiols]. The fluorescence intensity was recorded as the mutants were driven into different conformations using voltage jumps. Sugar binding and transport by the fluorophore-tagged mutants were blocked, but Na^+ binding and the voltage-dependent conformational transitions were unaffected. Structural models indicated that external Na^+ binding opened a large aqueous vestibule (600 $Å^3$) leading to the sugar-binding site. The fluorescence of TMR covalently linked to Y290C, T287C, and H83C decreased as the mutant proteins were driven from the inward to the outward open Na^+-bound conformation. The time courses of fluorescence changes (milliseconds) were close to the SGLT1 capacitive charge movements. The quench in rhodamine fluorescence indicated that the environment of the chromophores became more polar with opening of the external gates as the protein transitioned from the inward to outward facing state. Structural analyses showed an increase in polar side chains and a decrease in hydrophobic side chains lining the vestibule, and this was reflected in solvation of the chromophore. The results demonstrate the opening and closing of external gates in real time, with the accompanying changes of polarity of the sugar vestibule.

symporter | active site | conformation | voltage | tetramethylrhodamine

The intestinal sodium glucose cotransporter (SGLT1) is a member of the LeuT structural family of symporters and antiporters that are present in divergent gene families (e.g., LeuT, vSGLT, Mhp1, BetP, CaiT) (1). Emerging biochemical, biophysical, and structural studies suggest that these transporters share a common alternating access transport mechanism where the ligand-binding sites alternatively face the external or internal compartments. At present, the time course and nature of the conformational changes underlying ligand binding are poorly understood.

We have used functional site-directed fluorometry (2) to examine the conformational changes in human SGLT1 (hSGLT1) during discrete steps of the transport cycle. We and others have long used this approach to examine cotransporter conformational changes (e.g., refs. 3–6), but the difference here is that external fluorophores were introduced directly into the substrate-binding site. Basically, cysteine residues were introduced into the glucose-binding site and labeled with fluorophores, and changes in fluorescence intensity (ΔF) were monitored as the transporter was driven between the outward ($C2Na_2$ or C1) and inward (C6) conformations by voltage (Fig. 1).

The sugar-binding site is located in the middle of the hSGLT1 protein, and the rate of sugar entry and exit is determined by the opening and closing of external and internal gates (Fig. 1). Five residues within the sugar site were individually mutated to cysteine (Fig. 1*B*) and covalently labeled in the outward open conformation ($C2Na_2$) with tetramethylrhodamine (TMR)-thiols. For example, the mutants T287C and Y290C were labeled with MTS-TAMRA [2-((5(6)-tetramethylrhodamine)carboxylamino) ethyl methanethiosulfonate]. Sugar binding and transport by the labeled proteins were blocked, but the binding of external Na^+ ions to the Na1 and Na2 sites, as well as the conformational changes between the outward- and inward-facing conformations ($C2Na_2$ and C6), was relatively unperturbed.

Changes in the local environment of TMR covalently bound to the sugar-binding site were monitored and interpreted in terms of structural models. We conclude that changes in TMR fluorescence intensity are due to changes in solvent accessibility, caused by opening and closing of the outer hydrophobic gates (F453, F101, and L87), and the polarity of the TMR environment. The results also provide dynamic information about the structural changes in and around the sugar-binding site as the transporter alternates between outward ($C2Na_2$) and inward (C6) conformations.

Results

Mutants in the Glucose-Binding Site. Single cysteines were introduced into the sugar-binding site of hSGLT1 to attach environmentally sensitive fluorophores to monitor conformational changes between $C2Na_2$ and C6 in response to membrane potential (V_m) and Na^+ binding. The residues mutated were chosen from their location in the hSGLT1 homology model based on the crystal structure of vSGLT (7, 8) (Fig. 1*B*). The mutants were expressed in oocytes, and, except for N78C, the density of each mutant in the plasma membrane was similar to that of the wild-type (WT) hSGLT1, ~10^{10} molecules per oocyte (*SI Appendix*,

Significance

Site-directed fluorometry was used to understand conformational changes of the Na^+/glucose symporter. SGLT1 functions by a mechanism where the substrate-binding site alternates between the two faces of the membrane, but little is known about the underlying conformational changes. Rhodamines were covalently inserted into the substrate cavity, and changes of fluorescence were measured in real time with the opening and closing of the outer gate as SGLT1 was driven between inward and outward conformations using voltage jumps. Structural modeling indicated that the quenching with gating opening was due to an increased solvation of rhodamine and an increase in polar residues lining the wall of the cavity. This experimental approach will lead to a better understanding of the mechanism of membrane transport.

Author contributions: E.M.W. and D.D.F.L. designed research; E.G., B.A.H., and D.D.F.L. performed research; E.G., B.A.H., A.P., E.M.W., and D.D.F.L. analyzed data; and E.G., E.M.W., and D.D.F.L. wrote the paper.

Reviewers: F.B., The University of Chicago; and I.C.F., Florey Institute of Neuroscience and Mental Health.

The authors declare no conflict of interest.

[1]To whom correspondence may be addressed. Email: ewright@mednet.ucla.edu or dloo@mednet.ucla.edu.

This article contains supporting information online at www.pnas.org/lookup/suppl/doi:10.1073/pnas.1713899114/-/DCSupplemental.

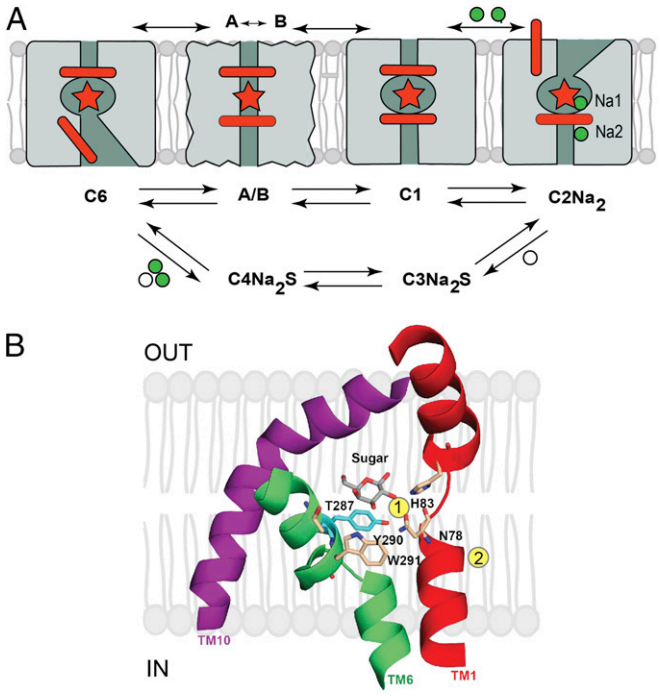

Fig. 1. (*A*) Kinetic model of Na^+/glucose cotransport by hSGLT1 emphasizing the five states shown in the absence of glucose (C6, A/B, C1, and $C2Na_2$). External Na^+ binds to the Na2 and Na1 sites in C1 to form the outward-facing conformation $C2Na_2$. SGLT1 has an apparent valence of 1, and in the absence of Na^+, V_m drives the protein between outward-facing C1 and inward-facing C6 through two intermediate states A and B. The rate of Na^+ binding is also voltage-dependent. At hyperpolarizing potentials (−150 mV), the protein is driven to $C2Na_2$, and at depolarizing potentials (+50 mV), it is driven to C6. The distribution of hSGLT1 between C6, C1, and $C2Na_2$ can be manipulated experimentally in a predictable manner by external Na^+ and V_m (e.g., at high external Na^+ at −150 mV, 100% of the protein is in $C2Na_2$, and at +50 mV, 100% of the protein is in C6). (*B*) Cartoon of hSGLT1 showing the location of the glucose-binding site and the Na1 and Na2 sites in an occluded inward-facing conformation showing the position of residues N78, H83, T287, Y290, and W291. The structural model was based on the X-ray structure of the bacterial homolog vSGLT in the inward-facing occluded conformation (8). T287, Y290, and W291 are on TM6. H83 and N78 are on TM1.

Table S1). There was a significant reduction in the apparent affinities [half-saturation concentration ($K_{0.5}$)] for glucose and Na^+ for N78C, H83C, Y290C, and W291C (8–10) (*SI Appendix*, Table S1). T287 is within the sugar-binding site, but the T287C mutation did not affect steady-state or pre–steady-state kinetics. All mutants exhibited voltage-dependent charge movements (Q) similar to WT with an apparent valence (z) of ∼1 and midpoint voltage ($V_{0.5}$) between +12 and −50 mV (9) (*SI Appendix*, Table S1).

Labeling of Cysteine Mutants. Four thiol reagents were used to label the cysteine mutants: 2-aminoethyl methanethiosulfonate (MTSEA), MTS-TAMRA, tetramethylrhodamine-6-maleimide (TMR6M), and tetramethylrhodamine-5-maleimide (TMR5M). Rhodamine was chosen because of its photostability and environmental sensitivity, and methanethiosulfonate (MTS) derivatives were preferred due to their efficient labeling of cysteine residues within the glucose-binding site (Table 1). Labeling was carried out in the presence of Na^+ as there was no labeling in the absence of external Na^+ (8). The extent of labeling was determined from the Na^+/sugar current (cotransport) induced by 100 mM α-methyl-D-glucopyranoside (αMDG) before and after exposure to the reagents (Table 1). MTSEA (0.1 mM for 2 min) inhibited sugar transport by N78C, H83C, T287C, and Y290C by more than 90%, but only by 20% for W291C (8, 11). Inhibition by MTS reagents was reversed by treatment of the oocytes with 10 mM DTT (not shown). There was no effect of thiol reagents on the WT transporter (8, 11).

TMR-thiol reagents (0.1 mM for 60 min) also inhibited sugar transport (Table 1), and the inhibition was reversed by DTT (not shown). MTS-TAMRA inhibited H83C, T287C, and Y290C by over 80%, but only by 45% and 10% for N78C and W291C, respectively. The maleimides were generally less effective (e.g., TMR5M only inhibited Y290C by 48%). In those cases of partial inhibition (Table 1), the subsequent treatment with MTSEA resulted in complete inhibition, indicating that the partial inhibition by TMR-thiols was due to restricted accessibility. Selectivity between TMR6M and TMR5M was noted for individual mutants (e.g., TMR5M was more potent than TMR6M for Y290C, T287C, and W291C, whereas TMR6M was a more potent inhibitor for H83C). Maleimide isomer selectivity suggests steric constraints on their access to cysteines in the aqueous vestibule of the sugar-binding site in $C2Na_2$. Molecular modeling of MTS-TAMRA covalently bound to mutants N78C, H83C, T287C, and Y290C indicated the fluorophores were in a vestibule lined by the outer regions of TM1, TM2, TM3, TM6, TM8, and TM10 (Fig. 2).

Although labeling of T287C and Y290C with MTS-TAMRA eliminated Na^+/glucose cotransport (Table 1), there was no effect on the voltage-dependent SGLT1 charge movements [i.e., there was no alteration of the voltage-dependent intermediate states between the open outward-facing sodium-bound state ($C2Na_2$) and the inward-facing empty state (C6)] (Fig. 1). *SI Appendix*, Figs. S1 and S2 show the Q/V curves, and *SI Appendix*, Table S2 gives the Boltzmann parameters for the WT and mutant transporters before and after labeling with MTS-TAMRA. There were no changes in maximal charge (Q_{max}), $V_{0.5}$, and z for Y290C and T287C. For H83C, there was no detectable charge movement after labeling, even though there were voltage-dependent fluorescent changes. For all three mutants, the kinetics of Na^+ binding to the fluorophore-labeled proteins were similar to those for the unlabeled proteins (*SI Appendix*, Table S3). There was no effect of 100 mM glucose on the charge movement recorded for labeled Y290C and T287C, indicating that labeling eliminated external sugar binding. For the WT transporter, sugar blocks charge movement with a dissociation constant (K_d) of 1 mM (12).

To summarize, labeling of Y290C, T287C, and H83C with MTS-TAMRA abolished sugar binding and transport but did not affect Na^+ binding to the Na1 and Na2 sites, or the conformation changes between C6 and $C2Na_2$, based on the recorded Q/V

Table 1. Inhibition of αMDG-induced current by MTSEA and rhodamine fluorescent dyes

	Inhibition, %			
Mutant	MTSEA	MTS-TAMRA	TMR5M	TMR6M
N78C	>90*	45 ± 5	20 ± 8	21 ± 5
H83C	98 ± 3	80 ± 3	10 ± 1	33 ± 8
T287C	91 ± 1	83 ± 7	27 ± 9	2 ± 8
Y290C	96 ± 4	92 ± 2	48 ± 2	13 ± 3
W291C	19 ± 5	9 ± 5	42 ± 12	15 ± 5

Oocytes expressing hSGLT1 mutants were clamped at −50 mV V_m, and the current induced by 100 mM αMDG was measured before and after incubation with the reagents. The percentage of inhibition of the current is shown as the mean ± SE of three to nine oocytes. The conditions of labeling were 2 min in 0.1 mM MTSEA in 100 mM Na^+ buffer and 1 h in 0.1 mM MTS-TAMRA, TMR5M, or TMR6M in 100 mM Na^+ buffer.
*From Sala-Rabanal et al. (8).

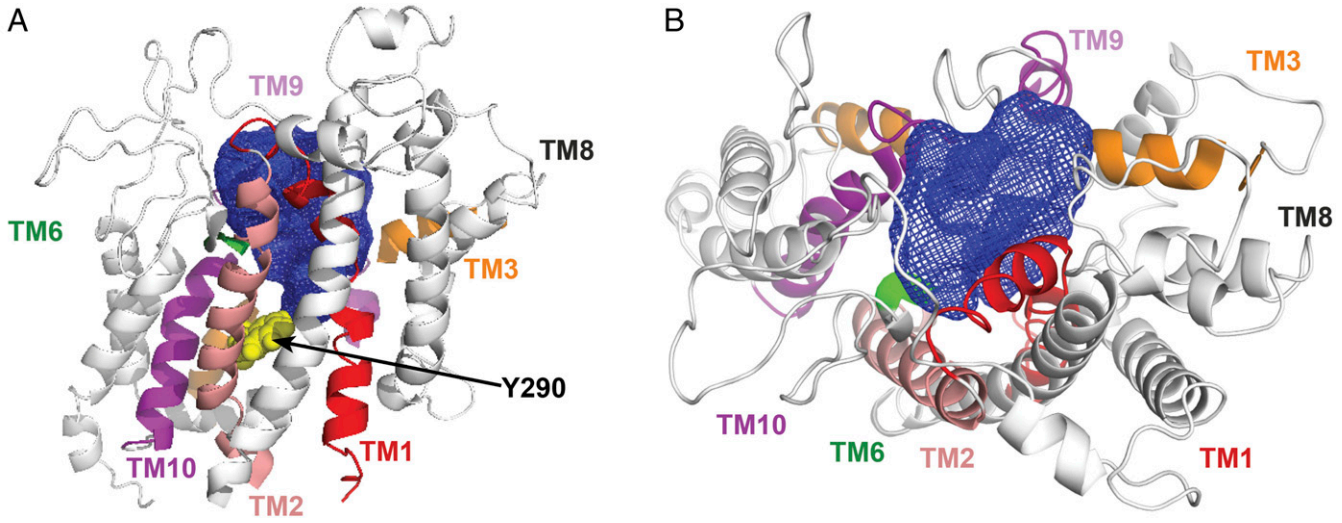

Fig. 2. External vestibule of hSGLT1. The space predicted to be occupied by MTS-TAMRA in the outward open conformation of hSGLT1 ($C2Na_2$) when covalently linked to Y290C, T287C, H83C, and N78C is shown. The volume of the space is 600 Å^3, and it is bounded by TM1, TM2, TM3, TM6, TM8, TM9, and TM10 with 57 side chains. Over 50% are aliphatic and small polar chains (Fig. 6 and *SI Appendix*, Figs. S6–S9). A side view (*A*) and a top view (*B*) are shown.

curves. The ΔF will report on voltage-dependent environmental changes in the sugar-binding pocket, even though incomplete labeling of N78C and W291C does not permit a correlation between charge and fluorescence changes.

Simultaneous Charge and Fluorescence Measurements. Fig. 3 shows a representative experiment with an oocyte expressing Y290C-SGLT1 labeled with MTS-TAMRA, where voltage-sensitive fluorescence was recorded in the presence and absence of external Na^+. The V_m was stepped from the holding potential (V_h) of −50 mV to a series of test values between −150 and +50 mV for 100 ms before returning to V_h (*SI Appendix*, Fig. S1). At −150 mV, SGLT1 is in the $C2Na_2$ conformation, and at +50 mV, it is in the C6 conformation. Following each ON and OFF voltage step, there was a change in the MTS-TAMRA-Y290C ΔF that approached a steady state with time constants in the millisecond range (Fig. 3 *A* and *B*). The ΔF decreased with hyperpolarizing voltage pulses and increased with depolarizing voltage pulses, and returned to baseline when V_m returned to V_h (i.e., there was a quench in TAMRA fluorescence as the hSGLT1 conformation transitioned from C6 to $C2Na_2$ and an increase in fluorescence when the protein transitioned from $C2Na_2$ to C6). The quench was larger and faster in Na^+ between C6 and $C2Na_2$ than between C6 and C1 in the absence of Na^+. As shown in Fig. 3 *B* and *D*, the time course of ΔF was slower than Q with depolarizing pulses. For hyperpolarizing pulses, ΔF was faster than Q in the presence of Na^+ and the time courses were similar in the absence of Na^+.

The steady-state ΔF vs. voltage (ΔF/V) and Q vs. voltage (Q/V) curves in the presence and absence of Na^+ (Fig. 3) followed Boltzmann relations. For ΔF/V, $V_{0.5}$ was −18 mV in Na^+ and −82 mV in its absence (*SI Appendix*, Fig. S1). The Q/V parameters were not substantially different from those before labeling (*SI Appendix*, Table S2). In the absence of Na^+, the Q/V curve with $V_{0.5}$ values shifted from −18 to −65 mV, as expected (9), and, again, the ΔF/V curve was superimposable (*SI Appendix*, Fig. S1*D*).

MTS-TAMRA fluorescence was sensitive to Na^+ (Fig. 3). The relationship between ΔF and [Na^+] was sigmoidal with a $K_{0.5}$ of 105 mM and a Hill coefficient of 1.5 (*SI Appendix*, Table S3), indicating two Na^+ ions interact with the labeled mutant protein at the Na1 and Na2 sites (Fig. 1). In contrast, addition of 100 mM αMDG in the presence of Na^+ had no effect on ΔF and Q (not shown), confirming that sugar does not interact with the fluorophore-derivatized protein.

To determine whether the quenching of rhodamine fluorescence in the transition from C6 to $C2Na_2$ was due to an increase in solvent accessibility, we tested whether or not collisional quenchers, such as acrylamide, Cs^+, or Cu^{++} in the external solution had any effect on fluorescence (13). Iodide was not used because we found that it interacts with the transporter. The approach was to measure ΔF of the MTS-TAMRA–labeled Y290C in the presence and absence of external 100 mM NaCl before and after exposure to NaCl or choline-Cl buffer containing 100 mM acrylamide, 10 mM CsCl, or 0.1 mM $CuCl_2$. No specific quenching of TAMRA was observed, even though these reagents quenched rhodamine fluorescence in aqueous solution (not shown and refs. 14, 15).

Variation in ΔF with Position of the Fluorophore in the Glucose-Binding Site. To further examine the motions near residue Y290, the mutant was labeled with TMR6M, which has a shorter link (by 3 Å) between cysteine and the chromophore (Fig. 4). When voltage was stepped from −90 mV to +50 mV, the time course of ΔF was faster for TMR6M than MTS-TAMRA. For TMR6M, the relaxation time constant (τ) was 4 ms for the ON transient and 3 ms for the OFF transient, while for MTS-TAMRA, τ was 10 ms for the ON and OFF responses. In addition, ΔF showed a fast transient (time to peak = 2 ms) for TMR6M-labeled Y290C in both the presence and absence of Na^+. Similar fast transients were observed for MTS-TAMRA T287C (discussed below). In the absence of Na^+, τ was slower for both dyes: for TMR6M, τ was 10 ms for the ON response and 4 and 20 ms for the OFF response, and for MTS-TAMRA, τ was 8 and 57 ms for the ON response and 13 and 100 ms for the OFF response. Thus, the two fluorophores monitored slightly different motions in the sugar-binding site. Since the MTS linker is longer than the maleimide linker by 3 Å, the two fluorophores are located at different positions (*Discussion*), and they may report different quenching kinetics. However, we cannot exclude the possibility that the fluorophore itself is changing the local motion of the protein.

We next examined the fluorescence changes with different mutants, T287C, N78C, and H83C, labeled with TMR. Fig. 5 shows the results with MTS-TAMRA-T287C. Similar to the

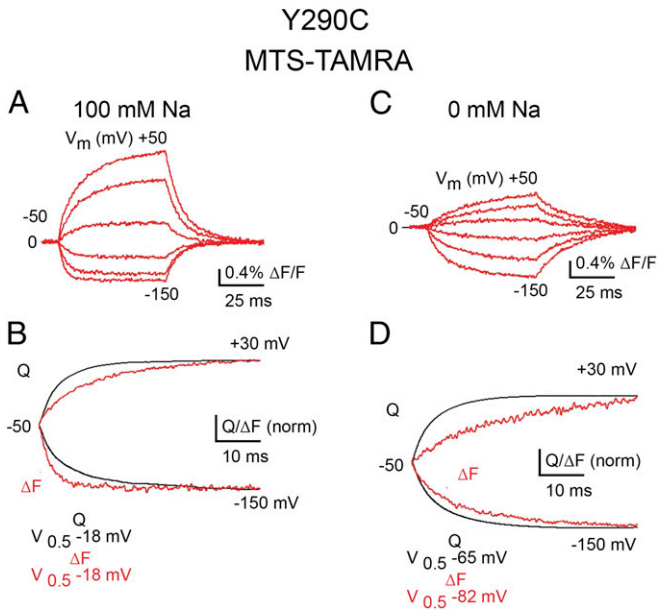

Fig. 3. Comparison between charge movement (Q) and fluorescence (ΔF) in the presence and absence of Na^+ for SGLT1-Y290C labeled with MTS-TAMRA. (*A* and *C*) Time courses of MTS-TAMRA ΔF for voltage jumps from the V_h (–50 mV) and to test voltages of +50, +10, –30, –90, –130, and –150 mV in the presence and absence of external 100 mM NaCl. (*B* and *D*) Simultaneous Q and ΔF changes for voltage steps from –50 mV to +50 and –150 mV. The pre–steady-state currents were isolated from the total current by subtraction of the capacitive and steady-state currents, and integrated to obtain Q at each voltage (*SI Appendix*, Fig. S1). The time constants for the hyper- and depolarizing pulses were similar in the presence and absence of Na^+ (7–10 ms). In external sodium, Y290C-hSGLT1 is in the $C2Na_2$ conformation at –150 mV and in the C6 conformation at +50 mV. In the absence of sodium Y290C-hSGLT1 is in the C1 conformation at –150 mV and in the C6 conformation at +50 mV (*SI Appendix*, Fig. S1). All of the data in this figure and *SI Appendix*, Fig. S1 were from a single oocyte. In *B* and *D*, Q and ΔF records are normalized (norm) to agree at the end of the pulse.

MTS-TAMRA– labeled Y290C, hyperpolarizing voltages decreased ΔF and depolarizing voltages increased ΔF. In contrast to Y290C, fast transients were observed with the onset of the voltage pulse (fast transients were also recorded for Y290C labeled with TMR6M; Fig. 4). Fig. 5*C* shows the ΔF records for 100-mV voltage jumps to +50 mV and −150 mV from −50 mV. ΔF decreased with hyperpolarization (Fig. 5*C*, black, −150 mV) and increased with depolarization (Fig. 5*C*, red, +50 mV). The submillisecond charge movements are not apparent ($\tau \sim 1$ ms). A comparison of the time course of charge transfer (integral of Q) and ΔF is shown in Fig. 5*B*. The time course of the slower charge movements closely follows ΔF, confirming the slow charge movements are associated with voltage-dependent conformational changes (4).

The fast transients for the ON and OFF responses are displayed at a higher time resolution to show their rise to peak (~2 ms) (*SI Appendix*, Fig. S3). These transients indicate fast kinetic steps in the conformation changes between $C2Na_2$ and C6, and between C1 and C6 (Fig. 1*A*). The difference in steady-state ΔF in the presence of Na^+ was greater than in its absence (Fig. 5 *C* and *D*), indicating that the conformational changes associated with Na^+ binding/dissociation ($C2Na_2 \rightleftarrows C1$) produce larger fluorescence changes than the transition between the empty (ligand-free) states C1 and C6 ($C1 \rightleftarrows C6$).

The steady-state ΔF and voltage (ΔF/V) curve for MTS-TAMRA-T287C (Fig. 5*A*) followed a Boltzmann relation, with a $V_{0.5}$ of −51 ± 1 mV and z of 0.6 ± 0.1 (*SI Appendix*, Fig. S2). The charge vs. voltage (Q/V) data were also fitted with a Boltzmann relationship, with a $V_{0.5}$ of −35 ± 1 mV and z of 0.6 ± 0.1 (*SI Appendix*, Fig. S2*B*). The T287C Q/V curves and Na^+ binding were not substantially different before and after labeling with MTS-TAMRA (*SI Appendix*, Tables S2 and S3).

Studies were extended to H83C and N78C labeled with MTS-TAMRA and TMR5M (*SI Appendix*, Figs. S4 and S5). For H83C labeled with MTS-TAMRA, even though there were no charge movements (*SI Appendix*, Table S2), the changes in ΔF with voltage in the presence or absence of Na^+ were similar to those for T287C and Y290C. Although the expression of N78C in the oocyte plasma membrane was only 10% of that for the WT and other mutants (*SI Appendix*, Table S1) and labeling was incomplete (Table 1), it was possible to record MTS-TAMRA fluorescence changes (*SI Appendix*, Fig. S5). The major differences for N78C-MTS-TAMRA were that that the polarity of ΔF was opposite to ΔF for T287C, Y290C, and H83C and there was a slow decline toward baseline ($\tau \sim 200$ ms).

Discussion

This study provides structural information about the glucose-binding site in the outward open ($C2Na_2$) and inward open (C6) conformations of hSGLT1, and the transitions between them (Fig. 1).

In a sugar transport cycle, two external Na^+ ions bind to the Na1 and Na2 sites of the empty transporter C1. Sugar then binds to the outward open Na^+-bound protein (in the $C2Na_2$ conformation). After external sugar binding ($C3Na_2S$), the glucose-binding site isomerizes ($C4Na_2S$) to release the sugar and two Na^+ ions into the cytoplasm (16). The cycle is completed by the return of the inward-facing empty protein (C6) to C1 via two transient intermediate conformations A and B. A single turnover of the protein in 20 ms results in the transport of two Na^+ ions and one sugar molecule from the outside to the inside.

There are three voltage-sensitive steps in the transitions between C6 and $C2Na_2$: (*i*) distribution of the apo-transporter between C6 and C1 with a charge of 0.7 and time constant in the range of 2–20 ms, (*ii*) external Na^+ binding (C1 to $C2Na_2$) with a charge of 0.3 and time constant 3–30 ms, and (*iii*) the intermediate transition from state A to B (A→B) at a low rate of 5 s^{-1} and a charge of 0.15 (9). State occupancy between C6 and $C2Na_2$ in the absence of sugar and internal ligands therefore depends on voltage and external Na^+ concentration. At saturating external Na^+

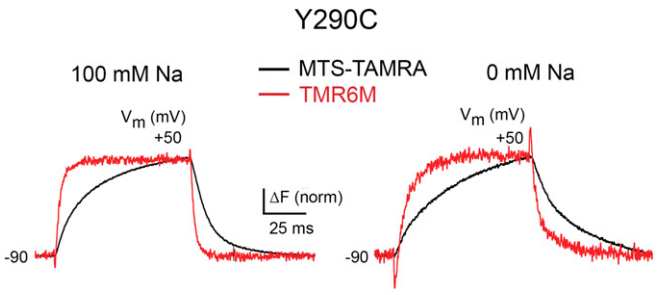

Fig. 4. Time course of the fluorescence changes for MTS-TAMRA and TMR6M attached to Y290C. Oocytes expressing hSGLT1 mutant Y290C were labeled with either MTS-TAMRA or TMR6M. The V_m was held at –90 mV, and the change in fluorescence (ΔF) was recorded on stepping V_m to +50 mV. After the fluorescence in 100 mM NaCl was recorded, the experiment was repeated in 100 mM choline-Cl (0 mM NaCl). The traces (black, MTS-TAMRA; red, TMR6M) have been normalized (norm) to agree at the end of the voltage pulse. The half-times for the TMR6M changes were faster in the presence and absence of Na^+ (4 and 10 ms) than those for MTS-TAMRA (10 ms and 8 and 57 ms). The ΔF/F signals were 0.39% for TMR6M and 4.74% for MTS-TAMRA. In 100 mM Na^+, 95% of the proteins were in the $C2Na_2$ conformation at –90 mV and 100% were in the C6 conformation at +50 mV, and in the absence of sodium, 80% of the proteins were in the C1 conformation at –90 mV and 100% were in the C6 conformation at +50 mV (*SI Appendix*, Fig. S1).

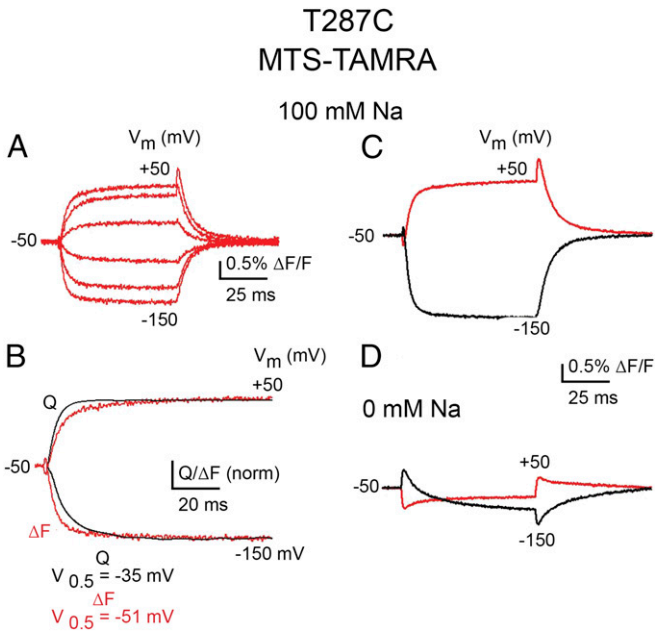

Fig. 5. Simultaneous recordings of voltage-induced charge movement (Q) and fluorescence (ΔF) for SGLT1-T287C labeled with MTS-TAMRA. A single oocyte expressing SGLT1-T287C labeled with MTS-TAMRA was held at −50 mV, and changes in ΔF were recorded in response to 100-ms step depolarizations (to +50 mV) and hyperpolarization (to −150 mV) in the presence of external Na^+ (100 mM NaCl). (*A*) Time course of the MTS-TAMRA ΔF changes. (*C*) For clarity, only two ΔF records are shown (at steps of +50 and −150 mV). (*B*) Time courses of simultaneous ΔF and Q for voltage steps of +50 and −150 mV. The traces have been normalized (norm) to agree at the end of the voltage pulse (100 ms). The time constants (τ) for the +50 mV pulse were 5 ms for Q and 10 and 75 ms for ΔF, and for the −150 mV pulses, they were 5 ms for Q and 4.5 and 75 ms for ΔF. (*D*) Time course of ΔF for voltage jumps to +50 and −150 mV in the absence of Na^+. Complete ΔF and Q/V curves are given in *SI Appendix*, Fig. S2.

and large hyperpolarizing voltages (−150 mV), the protein is in $C2Na_2$, and at depolarizing voltages (+50 mV), it is in C6 (*SI Appendix*, Figs. S1 and S2). A voltage pulse from −150 to +50 mV would result in a rapid transition of hSGLT1 from $C2Na_2$ to C6, and a rapid return to $C2Na_2$ at the end of the pulse. In the absence of Na^+, voltage pulses result in rapid transitions between C1 and C6 (Fig. 1).

According to hSGLT1 homology models, the underlying structural change in the transition from $C2Na_2$ to C6 is a 40° inward tilt of the outer half of TM10 and smaller inward movements of TM2 and TM8 (Fig. 6). In effect, the sugar-binding site in the absence of Na^+ is occluded from the external medium by an external barrier, possibly L87, F101, and F453, and external Na^+ binding opens this barrier to permit glucose binding (17). At present, there is no model of the C1 conformation.

We investigated the Na^+-induced conformational changes by measuring the access of the glucose-binding site to rhodamine thiols. Residues within the glucose-binding site were replaced with cysteine (N78C, H83C, T287C, Y290C, and W291C), and the mutants were expressed in oocytes. Four of the five introduced cysteines replaced residues coordinating sugar and, as expected, altered the apparent glucose and sodium affinities (8) (*SI Appendix*, Table S1). The fifth mutation, T287C, did not alter SGLT1 kinetics (*SI Appendix*, Table S1). Access of thiol reagents to the cysteines was determined from their effect on Na^+/glucose transport. MTS-TAMRA blocked sugar binding and transport by the H83C, T287C, and Y290C mutants (8) (Table 1 and *SI Appendix*, Tables S1 and S3), but only limited inhibition of N78C and W291C (Table 1). MTSEA treatment of N78C after MTS-TAMRA increased inhibition from 45 to 100%, indicating incomplete labeling by MTS-TAMRA. TMR-maleimides were less efficient in blocking sugar transport, but they were selective (Table 1). In some instances, TMR5M inhibited more than TMR6M; in other instances, TMR6M inhibited more than TMR5M. This indicates that there is steric hindrance to reagents reaching the cysteine mutants and is consistent with the selectivity of β-glucopyranoside binding to hSGLT1 (18).

Thiol regents only inhibited in the presence of external Na^+, and this, together with the lack of sugar and inhibitor binding in the absence of Na^+, shows that external Na^+ opens the external gate to the glucose-binding site. Molecular modeling of MTS-TAMRA covalently bound to Y290C, T287C, H83C, and N78C in the $C2Na_2$ conformation reveals that the aqueous vestibule is lined by the outer regions of TM1, TM2, TM3, TM6, TM8, and TM10 (Fig. 2). Most of the 57 side chains lining the vestibule on TM1 (n = 9), TM2 (n = 3), TM3 (n = 12), TM6 (n = 14), TM8 (n = 7), TM9 (n = 1), and TM10 (n = 11) are neutral aliphatic (40%) or aromatic (16%), with few charged groups (13%). Polar residues (mostly serines and threonines) account for 16% (Fig. 6 and *SI Appendix*, Figs. S6–S9). The volume of the vestibule is sufficient to accommodate rhodamine thiols (585 $Å^3$), phlorizin (389 $Å^3$), and a variety of large β-glucopyranoside substrates and inhibitors (18).

While MTS-TAMRA labeling of Y290C, T287C, and H83C blocked sugar transport, there was no dramatic effect on the kinetics of Na^+ binding (*SI Appendix*, Tables S1 and S3). There was also no effect on voltage-dependent charge movement (i.e., pre–steady-state kinetics) (*SI Appendix*, Figs. S1 and S2 and Table S2), indicating the voltage- and Na^+-dependent conformational changes between $C2Na_2$ and C6 are relatively unperturbed by the presence of the fluorophore.

In summary, site-directed fluorometry was used to probe the conformational transitions of SGLT1 between C6 and $C2Na_2$ through C1 (Fig. 1*A*). Caution is needed in extrapolating results from mutants to the native protein. However, in one case, T287C, there are minimal differences in Na^+ affinity and conformational changes between the TMR-labeled and WT SGLT1, based on the Q/V and τ/V relations. Since the results with T287C are representative of the other fluorophore-tagged proteins, we conclude that external Na^+ binding to the Na1 and Na2 sites opens the external gate to a large aqueous vestibule leading into the sugar-binding site, and that TMRs covalently attached within the sugar vestibule can be used to monitor transitions between C6, C1, and $C2Na_2$.

Analysis of Fluorescence Changes. In general, the quench in TMR fluorescence when the hSGLT1 transitions from an inward open (C6) to Na^+-bound outward open ($C2Na_2$) conformation is independent of the position of the dye in the glucose-binding site (Figs. 3–5 and *SI Appendix*, Figs. S4 and S5). Although the changes in TMR fluorescence can have many different causes, our hypothesis is that they are due to changes in solvation and the microenvironment of the fluorophore. This interpretation is based on structural analysis of TMR covalently linked to each of the mutants in the C6 and $C2Na_2$ conformations. The structural models of C6 and $C2Na_2$ were based on the inward-facing open conformation structure of vSGLT (34) and the outward open structure of the Mhp1 structural homolog (19) (*Materials and Methods*).

Consider first MTS-TAMRA covalently bound to Y290C in $C2Na_2$ (Fig. 6*A*). The dye is in an envelope created by TM helices 1, 2, 3, 6, 8, and 10, with the plane of the chromophore lying parallel and close to the outer helical end of TM10 (I456) and perpendicular to TM3. The residues within 6 Å of the chromophore and the solvent-accessible atoms are shown in a ligand-interaction diagram (20) (Fig. 6*D*). Notably, there are no polar residues within H-bonding distance or aromatic side chains

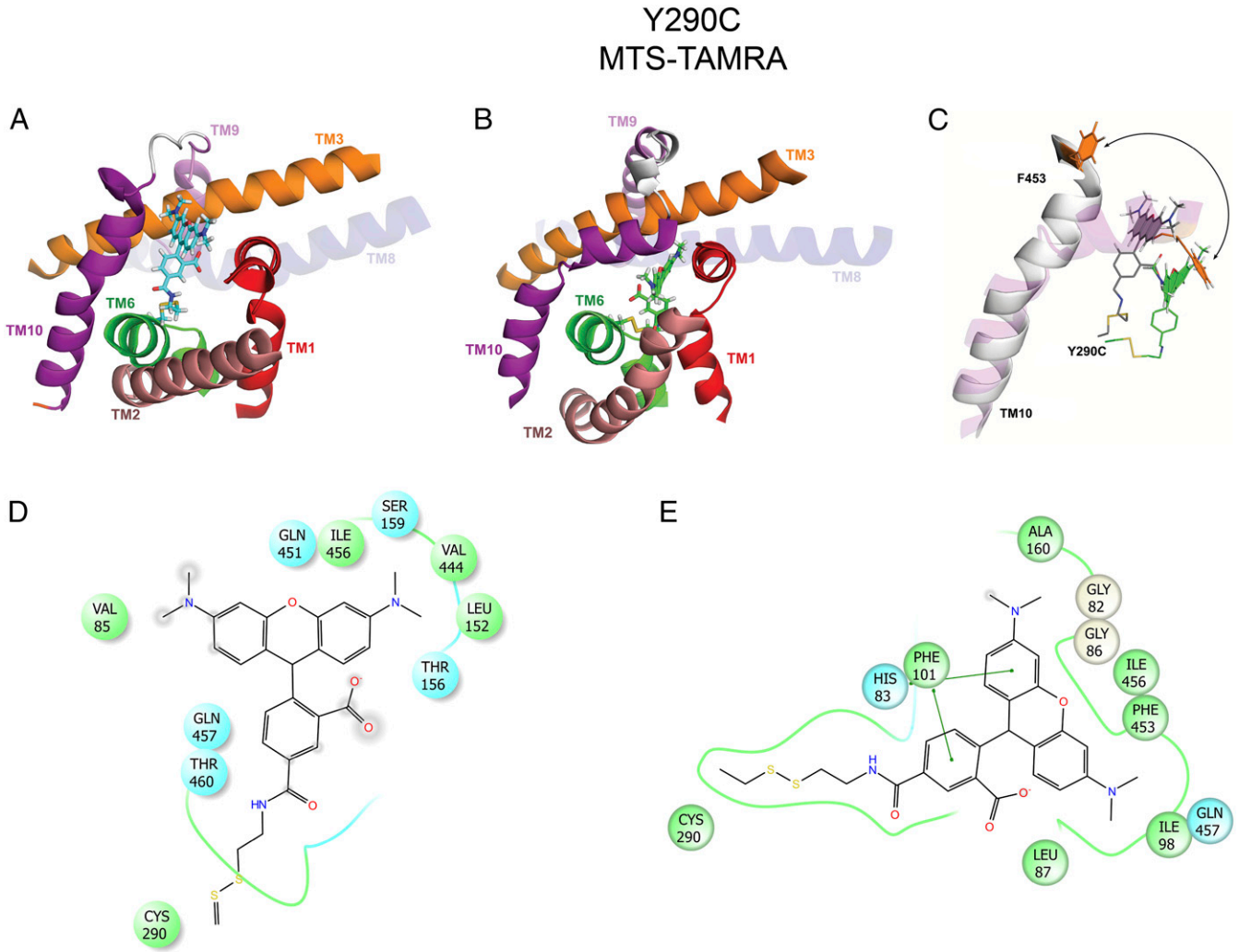

Fig. 6. Location of MTS-TAMRA linked to Y290C in the outward- and inward-facing conformations of hSGLT1. (*A* and *B*) Only TM1, TM2, TM3, TM6, TM8, TM9, and TM10 surround the dye in the C2Na2 and C6 conformations. (*C*) Major difference between the $C2Na_2$ and C6 states is the position of the outer half of TM10, which is clearly indicated. (*D* and *E*) Side chains within 6 Å of the chromophore in the outward open and inward occluded conformations are given. In the ligand interaction plots, residues in green are hydrophobic, those in cyan are polar, and those in white are glycine; chromophore atoms accessible to solvent are shown by a cloud. The green lines between F101 and the dye represent π-π stacking. The major difference is the accessibility of the chromophore to solvent upon closing of the outer gate (F453 shown in *C*).

capable of making π–π bonds with TMR, and the remainder of the residues have small hydrophobic side chains (V, L, and I). However, five of the tricyclic chromophore atoms are solvent-accessible.

In the inward-facing open conformation (C6), the major difference in conformation with $C2Na_2$ is the compaction of the sugar vestibule (Fig. 6*B*), due to the inward tilt of the outer half of TM10 and smaller inward motions of the outer segments of TM2 and TM8. As a result, TMR is now in a more hydrophobic microenvironment with the putative external gates (L87, F101, and F453) within 6 Å of the chromophore. F101 can make π–π bonds with the dye, but this would not contribute to an increase in fluorescence as F side chains are not efficient fluorescence quenchers (21–24). There is a paucity of W and Y side chains within 8–10 Å of the chromophore in both the $C2Na_2$ and C6 conformations, and so π–π stacking is not expected to contribute to rhodamine quenching. The most noticeable change is that there is a reduction in the number of chromophore atoms that are solvent-accessible (Fig. 6*E*). This suggests that the quenching of TMR fluorescence with the transition from C6 to $C2Na_2$ is due to the opening of the outer gate, an increase in solvent exposure, and a more hydrophilic microenvironment (compare Fig. 6 *D* and *E*). The same environmental changes may also account for the increase in TMR fluorescence with TAMRA-labeled T287C and H83C (Fig. 5 and *SI Appendix*, Figs. S6 and S7) and TMR6M-labeled Y290C (Fig. 4 and *SI Appendix*, Fig. S9).

When docked to Y290C, TMR6M is located in the space formed between TM1, TM3, and TM6, and the majority of the interactions with the transporter involve residues in these helices. This is in contrast to the MTS-TAMRA–labeled outward structure, where the fluorophore lies within the space between TM1, TM6, and TM10, and there are few interactions with residues in TM3. During the transition from the outward to inward conformation, both TMR6M and MTS-TAMRA move inward deeper into the vestibule, but tending to opposite directions. MTS-TAMRA moves slightly toward TM2 and TM7, whereas TMR6M moves slightly toward TM3 and closer to the discontinuous region of TM1 (Fig. 6 *A* and *B* and *SI Appendix*, Figs. S6–S9). TMR6M docked at Y290C is solvent-accessible in the outward conformation, and solvent accessibility is lost in the transition from the outward ($C2Na_2$) to inward (C6) conformation

(*SI Appendix*, Fig. S9 *A* and *B*). The increase in fluorescence is consistent with the decrease in solvation.

An exception is in the behavior of MTS-TAMRA-N78C, where there was a reverse in the polarity of the ΔF change from $C2Na_2$ to C6 (*SI Appendix*, Fig. S5). However, after the initial fast changes in fluorescence ($\tau = 2$ ms), there was a slow relaxation toward baseline ($\tau = 200$–300 ms); thus, in the steady state, no difference in fluorescence is to be expected.

There is an apparent inconsistency with the predicted solvent accessibility of the dyes in the outward open conformation in that we did not observe any quenching of TAMRA-Y290C by external collisional quenchers (e.g., Cs^+, Cu^{++}, acrylamide). Such quenchers are known to block MTS-TAMRA fluorescence of channels and transporters (6, 14, 15, 25), but the dyes were at the protein/aqueous interface in these cases. We suggest that in our case with the chromophore deep within the membrane protein, access is limited to water (11).

A further understanding of the mechanism of fluorescence quenching in theory could be obtained by recording the spectra, anisotropy, and lifetimes of the bound fluorophores in different conformations, but this is problematic because of the high background fluorescence [$\Delta F/F = 2.5\%$ compared with 15–20% with the *Shaker* K^+-channel (14, 15)].

Dynamics of Conformational Changes in the Sugar Vestibule. The time course of fluorescence changes (ΔF) closely followed charge movements between C6 and $C2Na_2$ (Figs. 3 and 5). The ΔF/V relation was similar to the Q/V relation, with similar $V_{0.5}$ values (*SI Appendix*, Figs. S1 and S2 and Table S2). Thus, the charge (Q) and fluorescence (F) at steady state report the same final conformational state distribution. In addition, since the total charge transferred and steady-state fluorescence changes (ΔF) are the sum of the individual partial charges and fluorescence changes, the similarity of the Q/V and ΔF/V relations indicates that the ratios of the charge transfers (z_{12}:z_{1A}:z_{AB}:z_{B6}) are similar to the ratios of relative quantum yields (qy_{12}:qy_{1A}:qy_{AB}:qy_{B6}). This also accounts for the similarity of the observed time course of ΔF, which is a weighted sum of products of relative quantum yields and changes of state occupancies, following a similar time course as Q, which is a weighted sum of the individual charges moved and the changes of transport occupancies. In general, the time constants of the fluorescence changes and the charge movement are not identical because the charge movement is a global property of the conformational change, while the fluorescence is local.

The time course of voltage-dependent fluorescence changes of TMR-thiols covalently bound to cysteine mutants in the Na^+/glucose-binding site reflects local interactions of the fluorophore and the transporter. There are two scenarios related to conformational changes between $C2Na_2$ and C6 and between C1 and C6. In both cases, there are multiple components: (*i*) fast transients in the submillisecond time domain, which are dye- and position-dependent (e.g., observed for Y290C-TMR6M and T287C-MTS-TAMRA but not for Y290C-MTS-TAMRA) (Figs. 4 and 5); (*ii*) intermediate with a time domain in the 5- to 10-ms range; and (*iii*) slow changes in the range of 30–600 ms (e.g., T287C-MTS-TAMRA) with ON time constants of 10, 75, and 340 ms and OFF time constants of 14 and 220 ms (not shown). In general, the time constants are larger in the absence of Na^+ than in its presence (Fig. 4 shows Y290C labeled with TMR6M and MTS-TAMRA). The multiple time constants are consistent with multiple steps between $C2Na_2$ and C6, but in the absence of structural information about these intermediates (e.g., C1, A/B), it is difficult to parse out the local interactions with the chromophores.

Fast Fluorescence Changes. Fast transient fluorescence changes, with a time to peak of 2 ms, were recorded in the presence and absence of Na^+ for some of the mutants. They were observed for some mutations labeled with one dye but not another (e.g., Y290C labeled with TMR6M but not TAMRA, T287C labeled with TAMRA) (Figs. 3–5). Simulations using our eight-state kinetic model (12) showed that the fluorescence transients can arise from a high-occupancy state, for instance, stepping membrane voltage from +50 to −50 mV, where the rate of the transition step (from $C_6 \rightarrow C_B$; Fig. 1*A*) is high. However, fast fluorescent transients could also have an electrochromic response due to the reorientation of the chromophore's transition dipole upon a step change in voltage. The magnitude of the electrochromic response depends on the orientation of the transition dipole in the local electric field. The fast component may therefore be a combination of a fast conformational transition and an electrochromic response.

The ΔF transients for ON and OFF voltage pulses were not apparently accompanied by transient charges, but this is due to the slow speed of the two-electrode voltage clamp, where the fast charge is buried in the membrane capacitance. We have previously measured submillisecond SGLT1 charge movements with the cut-open oocyte technique (4). The origin of the fast fluorescence transients between $C2Na_2$ and C6 and between C6 and C1 has not yet been clearly identified. However, in the inward conformation C6, the chromophore of TMR6M linked to Y290C interacts with the polar discontinuous region of TM1 (*SI Appendix*, Fig. S9*B*), and we hypothesize the fast fluorescence transients might be due to the motion of a voltage sensor in the region.

In summary, we have demonstrated that the sugar-binding site deep within hSGLT1 can be labeled selectivity with fluorescent dyes in the outward open conformation without seriously altering Na^+ binding or changing the time course of conformation changes between $C2Na_2$ and C6. The dyes, with a volume of 600 $Å^3$, lie within the sugar-binding vestibule, and their fluorescence closely followed the millisecond time courses of voltage-dependent conformational changes. Structural analysis of the proteins in the $C2Na_2$ and C6 conformations suggests that solvent accessibility to the chromophore determines fluorescence; namely, closure of the external gate, largely due to an inward tilt of TM10, reduces solvent accessibility. The time course of the fluorescence change follows the opening and closure of the external gate and the transitions of the ligand free transporter between the inward and outward states. The use of the fluorophores MTS-TAMRA and TMR6M located in different regions of the vestibule indicates motion of different time scales between the external surface of the vestibule and deeper into the vestibule near the discontinuous region of TM1.

Materials and Methods

Experimental Solutions and Reagents. TMR6M and TMR5M were purchased from Invitrogen-Molecular Probes. MTSEA and MTS-TAMRA were obtained from Toronto Research Chemicals. The TMRM isomer mixture was in a ratio of 60% TMR6M to 40% TMR5M. Stock solutions of the MTS (MTS-TAMRA and MTSEA) and maleimide reagents (TMR5M and TMR6M) were stored in dimethyl sulfoxide at −20 °C and diluted in NaCl buffer to the desired concentration immediately before the experiment. Concentrations of dimethyl sulfoxide did not exceed 1%. *Xenopus laevis* was purchased from Nasco. Enzymes were obtained from New England Biolabs. All other reagents were purchased from Sigma–Aldrich.

Oocytes were harvested from frogs as described previously under a protocol approved by the University of California, Los Angeles Chancellor's Committee on Animal Research (9). They were incubated in Barth's solution that contained 88 mM NaCl, 2.4 mM $NaHCO_3$, 1 mM KCl, 0.8 mM $MgSO_4$, 0.4 mM $CaCl_2$, 0.3 mM $Ca(NO_3)_2$, and 10 mM Hepes adjusted to pH 7.5 with Tris and supplemented with 10 mg/L gentamicin (Sigma), 5.8 mg/L ciprofloxacin (Bayer), and 50 mg/L streptomycin sulfate/50,000 U/mL penicillin G sodium (Invitrogen).

All experiments were performed in NaCl buffer [100 mM NaCl, 2 mM KCl, 1 mM $MgCl_2$, 1 mM $CaCl_2$, 10 mM Hepes adjusted to pH 7.5 with Tris] with or without αMDG. In experiments that required variations in the Na^+ concentration in the buffer, 0–100 meq/L NaCl was iso-osmotically replaced with choline-Cl.

Expression of Mutant hSGLT1 Transporters in *X. laevis* Oocytes. Cysteine mutations of residues in the sugar-binding site, N78C, H83C, T287C, Y290C, and W291C were expressed in oocytes as described (8, 9).

Electrophysiology. The two-electrode voltage clamp technique was used to control the V_m and monitor cotransport activity (3, 12, 26–28). Oocytes were normally bathed in 100 mM NaCl buffer, and a standard pulse protocol was applied, where V_m was normally held at −50 mV (V_h) and stepped to various test potentials (V_t from +50 mV to −150 mV in 20-mV decrements) for 100 ms before returning to V_h. The sugar-dependent current was the difference between the steady-state currents recorded in the presence and absence of sugar in the external NaCl buffer. For mutant T287C, we performed a steady-state kinetic analysis: Na^+ kinetics were determined from the 100 mM αMDG-dependent currents as a function of Na^+ concentration, and sugar (αMDG, glucose, and galactose) kinetics were determined from the 100 mM Na^+ currents as a function of sugar concentration. The data were fitted with

$$I = I_{max}[S]^n / (K_{0.5}^n + [S]^n), \quad [1]$$

where I and I_{max} are the current and maximal current, [S] is the external concentration of the substrate (Na^+ or sugar), n is the Hill coefficient, and $K_{0.5}$ is the half-saturation concentration (apparent affinity constant). For sugar kinetics, $n = 1$.

In the presence of Na^+ and absence of sugar, SGLT1 and mutants exhibited pre–steady-state currents (charge movements) with step jumps in membrane voltage (9, 29). The pre–steady-state current was obtained by fitting the total oocyte membrane current (I) to the equation:

$$I(t) = I_{cm} \exp(-t/\tau_{cm}) + I_{pss} \exp(-t/\tau) + I_{ss}, \quad [2]$$

where τ_{cm} and $I_{cm} \exp(-t/\tau_{cm})$ are the membrane bilayer capacitance with initial value I_{cm} and time constant τ_{cm}. I_{ss} is the steady-state current, and $I_{pss} \exp(-t/\tau)$ is the protein pre–steady-state current with initial value I_{pss} and time constant τ. The pre–steady-state charge movements (Q) for the ON and OFF transient currents were obtained by integrating $I_{pss} \exp(-t/\tau)$ as a function of time. Charge vs. voltage (Q/V) plots were fitted to a Boltzmann relation in the form:

$$(Q - Q_{hyp})/Q_{max} = 1/[1 + \exp\{(V_m - V_{0.5})zF/RT\}], \quad [3]$$

where $Q_{max} = Q_{dep} - Q_{hyp}$ (Q_{dep} and Q_{hyp} are the charges at depolarizing and hyperpolarizing limits, respectively), V_m is membrane potential, F is the Faraday constant, R is the gas constant, T is absolute temperature, $V_{0.5}$ is midpoint voltage, and z is the apparent valence of the voltage sensor. In this simple treatment, the Boltzmann relation is interpreted as the distribution of a moveable charge between two states, but we do recognize that charge distribution involves multiple components (4, 12). The number of transporters (N) in the plasma membrane was estimated from the formula $N = Q_{max}/z \cdot e$, where $z \approx 1$ for WT and SGLT1 mutants (9, 30), and e is the elementary charge. Q_{max} is proportional to the number of SGLT1 transporters in the plasma membrane: a Q_{max} of 10 nC is equivalent to 1×10^{10} proteins in the oocyte plasma membrane.

Chemical Modification of hSGLT1 Cysteine Mutants. The pre–steady-state transient and steady-state currents in NaCl buffer were recorded in the presence and absence of 100 mM αMDG before and after labeling with cysteine reagents. Oocytes were exposed to MTSEA (0.1 mM) for 2 min and to fluorophores MTS-TAMRA, TMR5M, and TMR6M (0.1 mM) for 1 h in the dark. The extent of alkylation was determined from the inhibition of the steady-state sugar-dependent current after treatment with the reagents, and is expressed as the percentage of inhibition of the αMDG current.

Voltage Clamp Fluorometry. Electrophysiological and fluorescence experiments were performed simultaneously on the same oocyte (3, 12, 27). For fluorescence experiments, the cysteine mutants were labeled for 1 h with a 0.1 mM concentration of the dyes (MTS-TAMRA, TMR5M, and TMR6M). The experiments were performed using the two-electrode voltage clamp on the stage of an inverted epifluorescence microscope. For measurements of fluorescence, the oocyte membrane was illuminated with a 150-W tungsten lamp and excitation and emission filters at 535 and 605 nm (XF33; Omega Optical). Fluorescence was monitored with a photodiode (1336-18BQ; Hamamatsu) connected to the camera port of the microscope. An electronic shutter was placed between the lamp and the preparation to minimize photobleaching. Fluorescence signals were amplified and low-passed at 500 Hz. The ΔF is expressed as arbitrary units. All experiments were performed at room temperature (20–22 °C). In each experiment, V_m was held at −50 mV and stepped to 11 voltages between +50 and −150 mV for 100 ms. For each voltage step, the fluorescence was recorded as the average for 10 runs. In those protocols with only two voltage steps, +50 and −150 mV, the fluorescence was the average of 100 trials. Data are expressed as ΔF and the voltage dependence, ΔF/V, was fitted to a single Boltzmann relation to compare with Q/V, even though ΔF is due to differences in the quantum yield of the bound fluorophore in multiple conformations between C6 and $C2Na_2$ (4, 12).

Data Analysis. Electrophysiological and fluorescence data were analyzed using pClamp 10 (Molecular Devices) and SigmaPlot 10 (Systat Software). On data obtained from a single oocyte, the statistics are given by the estimates and the SE of the fit. When data are from a population, the statistics are given by the means and the SEMs.

Homology Modeling and Docking. The coordinates for MTS-TAMRA and TMR6M were generated using the PRODRG server (31) and manually docked into hSGLT1 homology models using Coot (32). The Protein Data Bank (PDB) files were manually edited to introduce a disulfide bond between the cysteine mutants (H83C, N78C, T287C, and Y290C) and the MTS-TAMRA sulfur atom. Energy minimization was performed using UCSF Chimera (33), resulting in rmsd = 0.206 between the starting model and the minimized one.

The inward-facing open model for hSGLT1 (C6 conformation) was constructed by using a sequence alignment between hSGLT1 and vSGLT, and was threaded onto the inward-facing open conformation of vSGLT [PDB ID code 2XQ2 (34)] using the program Internal Coordinates Mechanics (Molsoft ICM-Pro-3.7-2c).

The outward-facing open Na^+-bound model ($C2Na_2$ conformation) of hSGLT1 was constructed based on the X-ray structure of the sodium-benzylhydantoin transporter Mhp1 in the outward open conformation [PDB ID code 2JLN (19)]. In the hSGLT1 model, the external end of TM6 tilted toward the middle of the opening of the substrate vestibule and obstructed glucose entry to the binding site. To resolve the problem, the model structure of TM6 was adopted from TM6 of the inward-facing occluded model of hSGLT1 based on vSGLT [PDB ID code 3DH4 (7)].

Protein–fluorophore interaction diagrams (20) between the covalently bound rhodamine reagents and the outward-facing ($C2Na_2$) and inward-facing (C6) conformations of the hSGLT1 homology models were constructed using Maestro Molecular Modeling Interface software and viewed in PyMol (Schrödinger, LLC).

ACKNOWLEDGMENTS. We thank Wendy Ravenhill for her computer graphic skills. This work was supported by NIH Grant DK19567, and E.G. was partially supported by a fellowship from the state of Navarra, Spain. A.P. was supported by NIH Grant GM078844.

1. Abramson J, Wright EM (2009) Structure and function of Na^+-symporters with inverted repeats. *Curr Opin Struct Biol* 19:425–432.
2. Priest M, Bezanilla F (2015) Functional site-directed fluorometry. *Adv Exp Med Biol* 869:55–76.
3. Loo DD, et al. (1998) Conformational changes couple Na^+ and glucose transport. *Proc Natl Acad Sci USA* 95:7789–7794.
4. Loo DD, Hirayama BA, Cha A, Bezanilla F, Wright EM (2005) Perturbation analysis of the voltage-sensitive conformational changes of the Na^+/glucose cotransporter. *J Gen Physiol* 125:13–36.
5. Virkki LV, Murer H, Forster IC (2006) Voltage clamp fluorometric measurements on a type II Na^+-coupled Pi cotransporter: Shedding light on substrate binding order. *J Gen Physiol* 127:539–555.
6. Patti M, Fenollar-Ferrer C, Werner A, Forrest LR, Forster IC (2016) Cation interactions and membrane potential induce conformational changes in NaPi-IIb. *Biophys J* 111: 973–988.
7. Faham S, et al. (2008) The crystal structure of a sodium galactose transporter reveals mechanistic insights into Na^+/sugar symport. *Science* 321:810–814.
8. Sala-Rabanal M, et al. (2012) Bridging the gap between structure and kinetics of human SGLT1. *Am J Physiol Cell Physiol* 302:C1293–C1305.
9. Loo DD, Jiang X, Gorraitz E, Hirayama BA, Wright EM (2013) Functional identification and characterization of sodium binding sites in Na symporters. *Proc Natl Acad Sci USA* 110:E4557–E4566.
10. Jiang X, Loo DD, Hirayama BA, Wright EM (2012) The importance of being aromatic: π interactions in sodium symporters. *Biochemistry* 51:9480–9487.
11. Zeuthen T, Gorraitz E, Her K, Wright EM, Loo DD (2016) Structural and functional significance of water permeation through cotransporters. *Proc Natl Acad Sci USA* 113: E6887–E6894.
12. Loo DDF, Hirayama BA, Karakossian MH, Meinild AK, Wright EM (2006) Conformational dynamics of hSGLT1 during Na^+/glucose cotransport. *J Gen Physiol* 128: 701–720.

13. Lakowicz JR (1999) *Principles of Fluorescence Spectroscopy* (Kluwer Academic/Plenum, New York), 2nd Ed.
14. Cha A, Bezanilla F (1997) Characterizing voltage-dependent conformational changes in the Shaker K^+ channel with fluorescence. *Neuron* 19:1127–1140.
15. Cha A, Bezanilla F (1998) Structural implications of fluorescence quenching in the Shaker K^+ channel. *J Gen Physiol* 112:391–408.
16. Adelman JL, et al. (2016) Stochastic steps in secondary active sugar transport. *Proc Natl Acad Sci USA* 113:E3960–E3966.
17. Wright EM, Loo DD, Hirayama BA (2011) Biology of human sodium glucose transporters. *Physiol Rev* 91:733–794.
18. Hirayama BA, Díez-Sampedro A, Wright EM (2001) Common mechanisms of inhibition for the Na^+/glucose (hSGLT1) and Na^+/Cl-/GABA (hGAT1) cotransporters. *Br J Pharmacol* 134:484–495.
19. Weyand S, et al. (2008) Structure and molecular mechanism of a nucleobase-cation-symport-1 family transporter. *Science* 322:709–713.
20. Wallace AC, Laskowski RA, Thornton JM (1995) LIGPLOT: A program to generate schematic diagrams of protein-ligand interactions. *Protein Eng* 8:127–134.
21. Marmé N, Knemeyer JP, Sauer M, Wolfrum J (2003) Inter- and intramolecular fluorescence quenching of organic dyes by tryptophan. *Bioconjug Chem* 14:1133–1139.
22. Mansoor SE, Dewitt MA, Farrens DL (2010) Distance mapping in proteins using fluorescence spectroscopy: The tryptophan-induced quenching (TrIQ) method. *Biochemistry* 49:9722–9731.
23. Jones Brunette AM, Farrens DL (2014) Distance mapping in proteins using fluorescence spectroscopy: Tyrosine, like tryptophan, quenches bimane fluorescence in a distance-dependent manner. *Biochemistry* 53:6290–6301.
24. Liao SM, Du QS, Meng JZ, Pang ZW, Huang RB (2013) The multiple roles of histidine in protein interactions. *Chem Cent J* 7:44.
25. Mannuzzu LM, Moronne MM, Isacoff EY (1996) Direct physical measure of conformational rearrangement underlying potassium channel gating. *Science* 271:213–216.
26. Hirayama BA, et al. (2007) Sodium-dependent reorganization of the sugar-binding site of SGLT1. *Biochemistry* 46:13391–13406.
27. Meinild AK, Hirayama BA, Wright EM, Loo DD (2002) Fluorescence studies of ligand-induced conformational changes of the Na^+/glucose cotransporter. *Biochemistry* 41: 1250–1258.
28. Chen E, West WC, Waters G, Caplan D (2006) Determinants of bold signal correlates of processing object-extracted relative clauses. *Cortex* 42:591–604.
29. Loo DD, Hazama A, Supplisson S, Turk E, Wright EM (1993) Relaxation kinetics of the Na^+/glucose cotransporter. *Proc Natl Acad Sci USA* 90:5767–5771.
30. Zampighi GA, et al. (1995) A method for determining the unitary functional capacity of cloned channels and transporters expressed in Xenopus laevis oocytes. *J Membr Biol* 148:65–78.
31. Schüttelkopf AW, van Aalten DM (2004) PRODRG: A tool for high-throughput crystallography of protein-ligand complexes. *Acta Crystallogr D Biol Crystallogr* 60: 1355–1363.
32. Emsley P, Cowtan K (2004) Coot: Model-building tools for molecular graphics. *Acta Crystallogr D Biol Crystallogr* 60:2126–2132.
33. Pettersen EF, et al. (2004) UCSF Chimera–A visualization system for exploratory research and analysis. *J Comput Chem* 25:1605–1612.
34. Watanabe A, et al. (2010) The mechanism of sodium and substrate release from the binding pocket of vSGLT. *Nature* 468:988–991.